Distinction between glioma progression and post-radiation change by combined physiologic MR imaging

Eiji Matsusue · James R. Fink · Jason K. Rockhill · Toshihide Ogawa · Kenneth R. Maravilla

Abstract

Introduction Magnetic resonance (MR) diffusion-weighted imaging (DWI), dynamic susceptibility contrast-enhanced perfusion imaging (DSC), and MR spectroscopy (MRS) techniques provide specific physiologic information that may distinguish malignant glioma progression from post-radiation change, yet no single technique is completely reliable. We propose a simple, multiparametric scoring system to improve diagnostic accuracy beyond that of each technique alone.

Methods Fifteen subjects with lesions suspicious for glioma progression following radiation therapy who had also undergone 3-tesla DWI, DSC, and MRS studies of the lesion were retrospectively reviewed. Minimum apparent diffusion coefficient (ADC) ratio, maximum regional cerebral blood volume (rCBV) ratio, and maximum MRS choline/creatine (Cho/Cr) and choline/N-acetyl-aspartate (Cho/NAA) metabolic peak-height ratios were quantified within each lesion. Each parameter (ADC ratio, rCBV ratio, and combined Cho/Cr and Cho/NAA ratios) was scored as either glioma progression (one point) or radiation change (zero point) based upon thresholds derived from our own data. For each lesion, the combined parameters yielded a multiparametric score (0 to 3) for prediction of tumor progression or post-radiation change.

Results Optimum thresholds for ADC ratio (1.30), rCBV ratio (2.10), and either combined Cho/Cr (1.29) and Cho/NAA (1.06) yielded diagnostic accuracies of 86.7%, 86.7%, and 84.6%, respectively ($p<0.05$). A combined multiparametric score threshold of 2 improved diagnostic accuracy to 93.3% ($p<0.05$).

Conclusion In this small series combining 3-T DWI, DSC, and MRS diagnostic results using a simple, multiparametric scoring system has potential to improve overall diagnostic accuracy in distinguishing glioma progression from post-radiation change beyond that of each technique alone.

Keywords Glioma · Radiation · Recurrence · MR diffusion · MR perfusion · MR spectroscopy

E. Matsusue · J. R. Fink · K. R. Maravilla
Department of Radiology, University of Washington,
1959 NE Pacific,
Seattle, WA 98195, USA

J. K. Rockhill
Department of Radiation Oncology, University of Washington,
1959 NE Pacific,
Seattle, WA 98195, USA

E. Matsusue (✉) · T. Ogawa
Division of Radiology,
Department of Pathophysiological and Therapeutic Science,
Faculty of Medicine, Tottori University,
36-1 Nishi-cho,
Yonago, Tottori 683-8504, Japan
e-mail: matsusue@grape.med.tottori-u.ac.jp

Introduction

Differentiation of post-radiation treatment effects from malignant glioma progression by gadolinium-enhancing magnetic resonance imaging (MRI) is confounded by overlap of findings. On anatomic MRI, corpus callosum involvement and multiple enhancing lesions may suggest recurrent tumor [1], while "soap bubble" or "Swiss cheese" patterns of enhancement may suggest radiation necrosis [2] but these are not robustly reliable. Both recurrent tumor and post-radiation change may exhibit changes at or near the original tumor site, including contrast enhancement, growth over time, mass effect, and surrounding edema.

Advanced MRI techniques, including diffusion-weighted imaging (DWI), dynamic susceptibility contrast-enhanced perfusion imaging (DSC), and MR spectroscopy (MRS), provide specific physiologic information about tumor

biology that is not available by conventional anatomic MRI alone. However, each of these techniques has limitations, and relatively few studies have examined whether combining multiparametric advanced MRI data can more reliably differentiate tumor progression from radiation change [3].

We performed a retrospective study of post-treatment brain tumor patients with MR imaging findings suggestive of either tumor progression or post-radiation change (confirmed by either histology or combined clinical and imaging follow-up) to determine whether combining advanced MRI studies using a simple, multiparametric scoring system could improve diagnostic accuracy in making this important distinction.

Methods

Patients

This study was approved for retrospective review of patient records by the IRB at our institution. All post-treatment patients with cerebral gliomas who underwent 3-T MRI that included DWI, DSC, and MRS at the same follow-up evaluation at our institution between October 2006 and September 2007 with technically interpretable results in at least two of these three parameters were identified. Review of medical records and conventional MR images identified

21 adult patients who met the following inclusion criteria: prior surgery for glioma followed by radiation treatment with external-beam radiation therapy and/or gamma knife radiosurgery and development of a new enhancing lesion or progressive T2 growth within the radiation field on post-treatment follow-up MR images.

Of these 21 potential subjects, 15 patients (nine men and six women; mean age, 46.9 years; age range, 30–64 years; glioma histology, WHO grade II ($n=9$), III ($n=1$), or IV ($n=5$)) had confirmed final diagnoses of either tumor progression or post-radiation change; in six patients, a final diagnosis could not be determined from available information. Clinical information is given in Table 1. Final determination between tumor progression and post-radiation change was decided either histologically (three cases) or through combined clinical and imaging follow-up (12 cases) using the following criteria: Lesions were classified as radiation change if they (1) disappeared or decreased in size on subsequent MR examination or (2) were present but unchanged in serial follow-up MR examinations for 6 months or longer without receiving any further therapy. If an enhancing lesion increased in size on at least two serial MR examinations over 2 months or more, it was interpreted as tumor progression. Seven cases of tumor progression and five cases of post-radiation change were thus determined clinicoradiologically. In all cases the time interval from physiologic imaging studies to final diagnosis ranged between 6 and

Table 1 Clinical information.

Case no.	Age/Sex	Final diagnosis	Histology of the primary tumor	Location	Operation	Radiation type	Dose (Gy)	Chemo therapy	Interval between radiation therapy and appearance of lesion (month)
1	48/F	Radiation change	Astrocytoma (grade II)	R FL	STR	EBRT	?	None	254
2	41/M	Radiation change	Low-grade glioma (grade II)	L FL	STR	EBRT	54	None	3
3	45/M	Radiation change	Ependymoma	4th ventricle	STR	EBRT+SRS	56+18	Etoposide	116
4	30/M	Radiation change	Glioblastoma	L FL	STR	EBRT+SRS	?	T+C	24
5	43/M	Radiation change	Glioblastoma	R PL	STR	EBRT	60	T+C	16
6	30/F	Tumor recurrence	Low-grade glioma (grade II)	L FL	SBB	EBRT	54	None	40
7	39/M	Tumor recurrence	Astrocytoma (grade II)	R FL	STR	EBRT	54	T+C	17
8	49/M	Tumor recurrence	Astrocytoma (grade II)	L FL	STR	EBRT+SRS	?	T	7
9	48/F	Tumor recurrence	Oligodendroglioma	L caudate nucleus	SBB	EBRT+SRS	54+18	T+CPT-11	6
10	64/M	Tumor recurrence[a]	Low-grade glioma (grade II)	R TL	GTR	EBRT	58	None	8
11	37/M	Tumor recurrence[a]	Astrocytoma (grade II)	R TL	STR	EBRT	?	T	156
12	54/M	Tumor recurrence	Anaplastic astrocytoma	L TL	SBB	EBRT	59	T	15
13	55/F	Tumor recurrence	Glioblastoma	R FL	STR	EBRT+SRS	?	T	4
14	59/F	Tumor recurrence	Glioblastoma	L PL	SBB	EBRT	61	T	17
15	61/F	Tumor recurrence[a]	Malignant glioma	L PL	STR	EBRT	60	T	14

FL frontal lobe, *PL* parietal lobe, *TL* temporal lobe, *R* right side, *L* left side, *STR* subtotal resection, *GTR* gross total resection, *SBB* stereotactic brain biopsy, *EBRT* external-beam radiotherapy, *SRS* stereotactic radiosurgery, (?) radiation dose details not available, *T* temozolomide, *C* carboplatin

[a] Final diagnosis was histologically proved by surgical resection or stereotactic biopsy. Cases 10 and 11 were diagnosed as anaplastic astrocytoma and case 15 as gliosarcoma

15 months (mean 11.2 months) in radiation change and 1 to 11 months (mean 4.8 months) in tumor progression cases.

Data acquisition

MR imaging in all 15 subjects was performed using the same 3-T clinical MR system (Philips Achieva, Best, The Netherlands) with an eight-channel phased array head coil.

Conventional MR imaging sequences included axial spin-echo T1 (TR/TE=400/10 ms) pre- and post-contrast, axial turbo spin-echo T2 (TR/TE=3,000/90 ms), and axial fluid-attenuated inversion recovery (FLAIR) images (TR/TE/TI=11,000/125/2,800 ms) all with slice/gap=5/0 mm, FOV=230 mm.

DWI

DWI utilized spin-echo echo-planar sequence (TR/TE= 5,210/53 ms, echo planar imaging (EPI) factor=77, FOV = 230 × 150 mm, slice/gap=4/1 mm, excitations=1, matrix 112×89, slice number=28, acquisition time 32 s). DW images were acquired using b values of 0 and 1,000 s/mm^2. Apparent diffusion coefficient (ADC) maps were calculated from the DW images.

DSC

DSC was performed during the first pass of a bolus of gadobenate dimeglumine (MultiHance, Bracco Diagnostics, Princeton, NJ, USA) using a 3D shifted-echo multishot, echo-planar MR imaging sequence, principles of echo shifting with a train of observations (PRESTO), effective TR/TE=16/ 24 ms; flip angle=7°; FOV = 230 × 187 × 120 mm, matrix = 128 × 108 × 40, and acquisition voxel size = 3.6 × 3.6 × 3 mm (reconstructed voxel size = 1.8 × 1.8 × 3 mm). A series of 50 multisection acquisitions was acquired at 1.4-s intervals. Ten baseline acquisitions were acquired before contrast injection. A 20-ml contrast bolus was administered followed by a 20 ml saline flush at 5 ml/s using a power injector (Spectris MR injector, MedRad, Indianola, PA, USA).

Following DSC acquisition, a high-resolution, 3D magnetization prepared rapid gradient echo sequence was done for coregistration to the DSC slice position and angulation using the same FOV with following parameters: TR/TE/MP=7/3.2/850 ms, flip angle=8°.

MRS

Proton MR spectra were acquired after administration of contrast in all cases. Multivoxel proton MRS (chemical-shift imaging) with TE of 144 and/or 288 ms and TR of 2,000 ms, FOV=24 cm, was used for MRS studies in all cases. For multivoxel MRS, the voxel size was 1.0× 1.0 × 1.2 cm^3. Automated shimming and water suppression

were used. Signal contamination from fat tissue in the skull and skull base was avoided by using spatially localized saturation bands to suppress signal from scalp or orbital fat on multivoxel MRS. Acquisition time for spectroscopic imaging studies varied between 5 and 7 min. If multivoxel MRSI resulted in poor-quality spectra due to magnetic field inhomogeneities, then single-voxel MRS (TR/TE=2,000/36; 128 averages) was performed. For all MRS acquisitions, the volume of interest (VOI) was manually placed on either FLAIR images or contrast-enhanced axial T1-weighted images. For single-voxel MRS, the volume of the VOI was adapted to the size and extent of the lesion, resulting in voxel sizes ranging from 1.1 × 1.1 × 1.3 to 1.5 × 1.9 × 2.0 cm^3.

Data evaluation

Review of DWI, DSC, and MRS studies was performed on an independent workstation (Philips, Extended Workspace, Best, The Netherlands) by a single experienced neuroradiologist (E.M.). Pre- and post-contrast T1-weighted, T2-weighted, and FLAIR images were accessible during analysis of advanced MR imaging data.

DWI

Minimum ADC measurements were obtained by identifying regions of lowest ADC values determined from regions of interest (ROIs) placed within lesion, taking care that ROIs were not placed over areas of susceptibility. ROI size ranged from 3 to 15 mm^2, depending on lesion size. ADC values from ROI within normal-appearing white matter (judged as normal on all T2-weighted, FLAIR, and contrast-enhanced T1-weighted images) were used to calculate ADC ratio(ADC [lesion]/ADC [contralateral white matter]). Whenever possible, control white matter ROIs were placed in the mirror image location in the contralateral hemisphere.

DSC

Unprocessed DSC perfusion images were evaluated to ensure that ROIs were not placed over blood vessels. Highest relative cerebral blood volume (rCBV) measurements were obtained by ROI placement in regions of maximal rCBV. ROI size ranged from 3 to 15 mm^2. Normal-appearing white matter ROIs were placed similar to that previously described, and an rCBV ratio(rCBV [lesion]/rCBV [contralateral white matter]) was then determined.

MRS

For multivoxel MRS, spectra from individual voxels within the lesion were analyzed. After baseline correction, peaks were

measured for choline (Cho), 3.21 ppm; creatine (Cr), 3.02; and *N*-acetyl aspartate (NAA), 2.01 ppm. Metabolite ratios were calculated based on peak-height measurements for each metabolite. All spectroscopic data from either multi- or single-voxel MRS were expressed as intralesional metabolite ratios. For multivoxel MRS, the single voxel in the lesion with the highest Cho/Cr and Cho/NAA ratios was selected.

Statistical analysis

The mean and standard deviation and minimum and maximum value of the ADC ratio, rCBV ratio, Cho/Cr ratio, and Cho/NAA ratio were calculated using Excel 2000 (Microsoft, Redmond, WA, USA). Mann–Whitney U tests were used to evaluate differences in each of these ratios between subjects classified as tumor progression and subjects classified as post-radiation change.

Threshold points that provided the best combination of sensitivity and specificity for each parameter were selected using ROC analysis. We determined the accuracy, sensitivity, specificity, positive predictive value, and negative predictive value of each parameter using Chi-square analysis.

Multiparametric scoring system

All cases were scored as either 0 (post-radiation change) or 1 (tumor progression) for each parameter (ADC ratio,

rCBV ratio, and metabolic ratios) according to its threshold. These individual scores were summed for each subject, yielding a combined score between 0 and 3 for each case. If the combined score was 0 or 1, the lesion was classified by multiparametric scoring as post-radiation change; if the sum was 2 or 3, the lesion was classified as tumor progression. Finally, we calculated the accuracy, sensitivity, specificity, positive predictive value, and negative predictive value of the above multiparametric scoring system using Chi-square analysis (level of significance, $p<0.05$).

Results

All 15 patients underwent combined 3-T DWI, DSC, and MRS; however, in two patients, MRS was uninterpretable due to technical failure. Results are summarized in Table 2.

ADC ratio, rCBV ratio, and metabolic ratios

ADC ratio, rCBV ratio, and metabolic peak-height ratios in all cases are summarized in Table 3. Representative MR images and MRS for tumor progression are shown in Fig. 1. ADC ratios were lower in tumor progression (0.75–1.30, mean 1.14±0.18) than in post-radiation change (1.29–2.06, mean 1.57±0.35). However, one case (case 4) with post-radiation change demonstrated marginally low ADC ratio (1.29;

Table 2 MRI (diffusion, perfusion, and spectroscopic imaging) and scoring analysis of post-radiation therapy.

Case no.	Final diagnosis	Time interval (months)	ADC ratio	ADC scoring	rCBV	rCBV scoring	MRS				Scoring sum
							TE	Cho/Cr	Cho/NAA	MRS scoring	
1	Radiation change	15	1.33	0	1.56	0	N/A	N/A	N/A	N/A	0 or 1
2	Radiation change	13	2.16	0	2.06	0	144	0.64	0.72	0	0
3	Radiation change	10	1.50	0	2.02	0	N/A	N/A	N/A	N/A	0 or 1
4	Radiation change	12	1.29	1	2.81	1	37	1.86	2.21	1	3
5	Radiation change	6	1.58	0	0.64	0	144	0.84	0.56	0	0
6	Tumor recurrence	11	0.75	1	3.79	1	36	2.03	1.68	1	3
7	Tumor recurrence	11	0.99	1	3.01	1	144	2.16	1.18	1	3
8	Tumor recurrence	2	1.26	1	3.00	1	39	1.88	1.38	1	3
9	Tumor recurrence	4	1.24	1	2.47	1	144	1.69	1.06	1	3
10	Tumor recurrence	1	1.30	1	4.20	1	288	1.87	1.10	1	3
11	Tumor recurrence	4	1.11	1	1.99	0	37	1.29	1.38	1	2
12	Tumor recurrence	2	1.5	0	4.77	1	36	2.64	3.69	1	2
13	Tumor recurrence	3	1.29	1	2.10	1	288	2.02	1.67	1	3
14	Tumor recurrence	2	1.06	1	2.57	1	144	1.34	1.78	1	3
15	Tumor recurrence	8	1.30	1	5.40	1	144	1.76	0.72	0	2

ADC ratio scoring: ADC ratio $\leqq 1.30$, scoring 1; ADC ratio >1.30, scoring 0. rCBV ratio scoring: rCBV ratio $\geqq 2.10$, scoring 1; ADC ratio <2.10, scoring 0. MRS scoring: Cho/Cr $\geqq 1.29$ and Cho/NAA $\geqq 1.06$, scoring 1; Cho/Cr <1.29 and Cho/NAA <1.06, scoring 0. Scoring sum: ADC ratio score+rCBV ratio score+MRS score

Time interval time interval from evaluation of physiologic imaging studies to final diagnosis

Table 3 ADC ratio, rCBV ratio, and metabolic ratios in radiation change and tumor recurrence.

	Radiation change		Tumor recurrence		p value
	Range	Mean±SD	Range	Mean ± SD	
ADC ratio	1.29–2.16	1.57±0.35	0.75–1.30	1.14±0.18	<0.05
rCBV ratio	0.64–2.81	1.82±0.79	1.99–4.77	3.33±1.16	<0.05
Cho/Cr	0.64–1.86	1.11±0.66	1.29–2.64	1.87±0.39	NS
Cho/NAA	0.56–2.21	1.16±0.91	0.72–3.69	1.56±0.82	NS

NS no significance

Fig. 2), and one case (case 12) with tumor progression showed relatively high ADC ratio (1.50).

rCBV ratios were higher in tumor progression (1.99–4.77, mean 3.33±1.16) than in post-radiation change (0.64–2.81, mean 1.82±0.79). However, one case (case 4) with post-radiation change demonstrated relatively high rCBV ratio (2.81; Fig. 2), and one case (case 11) with tumor progression showed relatively low rCBV ratio (1.99).

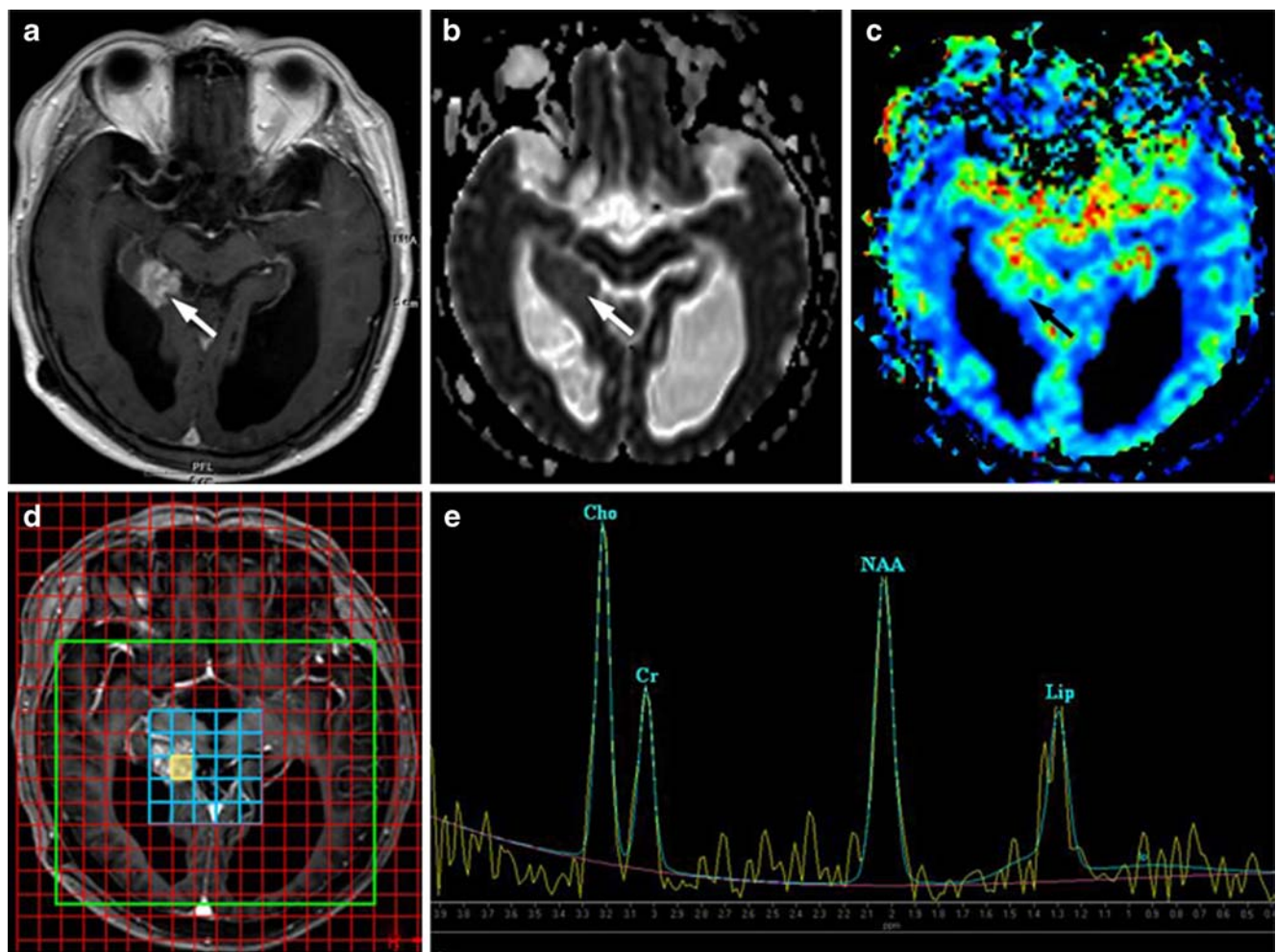Cho/Cr ratios were higher in tumor progression (1.29–2.64, mean 1.86±0.37) than in radiation change (0.64–1.86,

Fig. 1 A 64-year-old man who underwent surgery and radiation therapy for low-grade glioma in right temporal lobe (case 10). **a** T1-weighted image obtained after gadolinium administration shows focal nodular enhanced area in the medial temporal lobe. **b** ADC map shows intermediate intensity of arrowed area (ADC ratio, 1.30). **c** Relative cerebral blood volume map shows increased rCBV in the arrowed area (rCBV ratio, 4.20). **d** Volume of interest (*yellow square*) for multivoxel MRS was placed over the arrowed area. **e** Spectra show increased Cho/NAA and Cho/Cr ratios, 1.87 and 1.10, respectively. Increased lipid peak is also seen. These findings seen on ADC map, rCBV map, and MRS were consistent with tumor recurrence. Histopathology from repeat surgical specimen revealed anaplastic astrocytoma
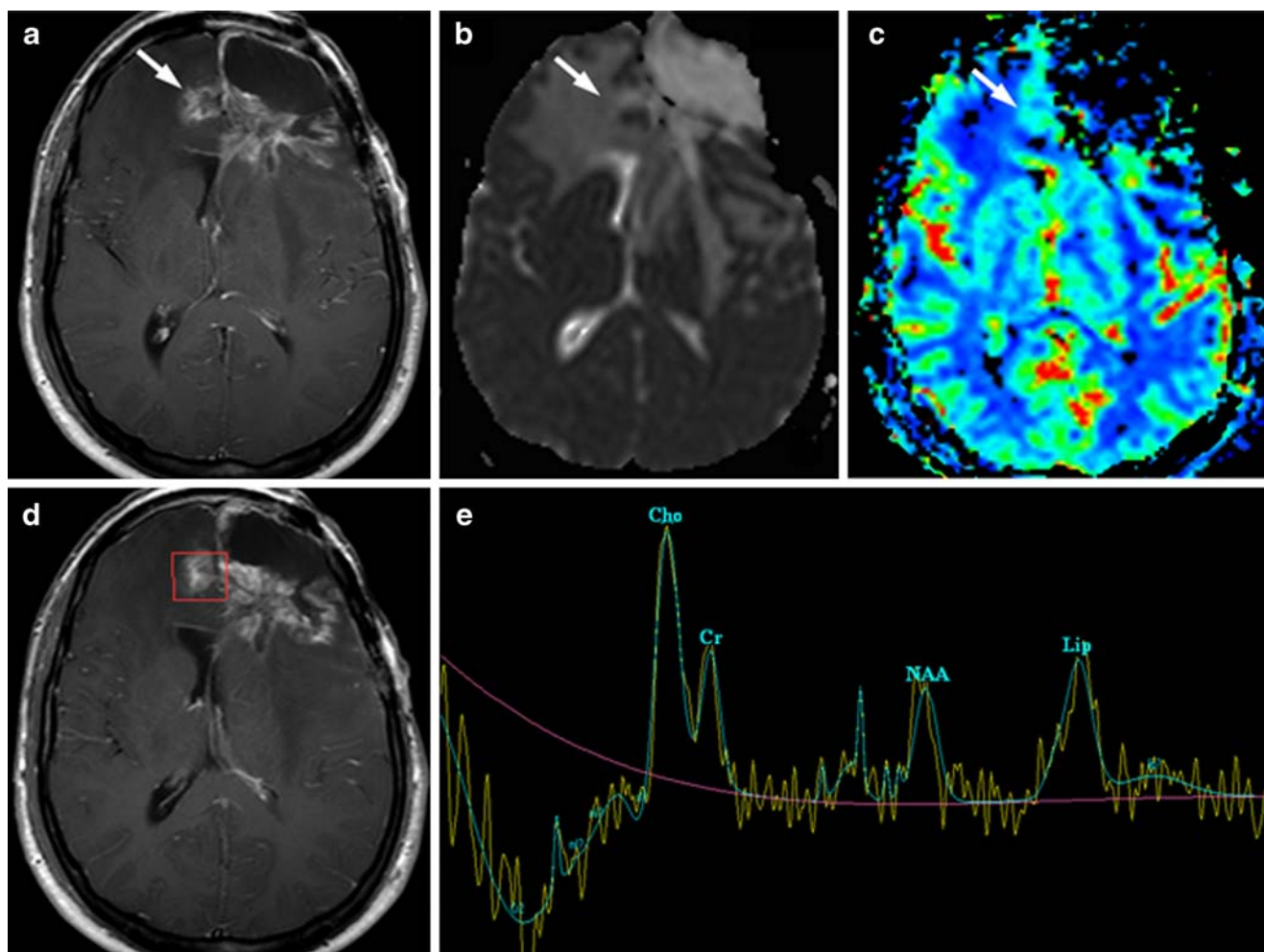
Fig. 2 A 30-year-old man who underwent surgery and radiation therapy for glioblastoma in frontal lobe (case 4). **a** T1-weighted image obtained after gadolinium administration shows widespread enhanced area involving residual left frontal lobe as well as arrowed right frontal lobe. **b** ADC map shows intermediate intensity of arrowed area (ADC ratio, 1.29) and widespread hyperintensity in the bilateral frontal white matter and internal, external, and extreme capsule, suggesting vasogenic edema. **c** Relative cerebral blood volume map shows increased rCBV in the arrowed area (rCBV ratio, 2.81). **d** Volume of interest for single-voxel MRS was placed over the arrowed area. **e** Spectra show pathologic spectra with increased Cho/NAA and Cho/Cr ratios, 1.86 and 2.21, respectively. Increased lipid peak are also seen. These findings seen on ADC map, rCBV map, and MRS were consistent with tumor recurrence although subsequent studies showed no progression of lesion on MRI, and the enhanced area was unchanged 12 months later, suggesting radiation change

mean1.11 ± 0.66), although one case (case 4) with radiation change showed relatively high Cho/Cr ratio (1.86; Fig. 2).

Cho/NAA ratios were higher in tumor progression (0.72–3.69, mean 1.56 ± 0.82) than in radiation change (0.56–2.21, mean 1.16 ± 0.91). However, one case (case 4) with radiation change demonstrated relatively high Cho/NAA ratio (2.21; Fig. 2), and one case (case 15) with tumor progression showed relatively low Cho/NAA ratio (0.72; Fig. 3).

ADC ratio and rCBV ratio differences between radiation change cases and tumor progression cases were both statistically significant ($p<0.05$, Mann–Whitney U test). However, in this small series Cho/Cr ratio and Cho/NAA ratio differences between radiation change cases and tumor progression cases were not statistically significant.

Performance of individual parameters

We adopted the threshold points that provided the best combination of sensitivity and specificity. The thresholds selected were ADC ratio greater than 1.30, rCBV ratio greater than 2.10, Cho/Cr greater than 1.29, and Cho/NAA greater than 1.06, resulting in overall diagnostic accuracies of 86.7%, 86.7%, and 84.6%, for DWI, DSC, and MRS, respectively ($p<0.01$, Chi-square test).

Performance of the semi-quantitative scoring system

If ADC ratio was 1.30 or less, the score was regarded as 1; if more than 1.30, the score was 0. If rCBV ratio was 2.10
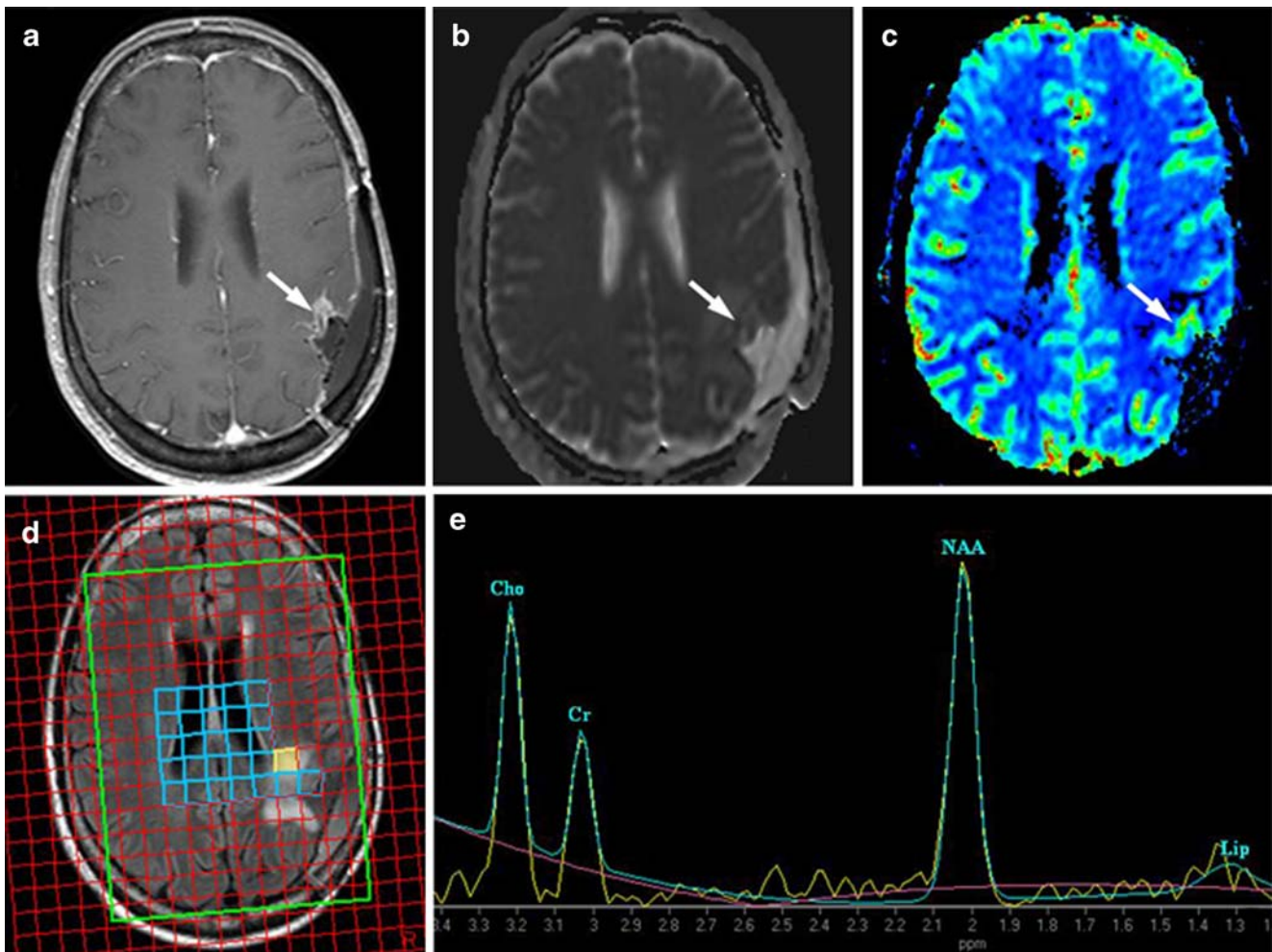
Fig. 3 A 61-year-old woman who underwent surgery and radiation therapy for high-grade glioma in left parietal lobe (case 15). **a** T1-weighted image obtained after gadolinium administration shows focal cortical enhanced area in the residual parietal lobe. **b** ADC map shows intermediate intensity of arrowed area (ADC ratio, 1.30). **c** Relative cerebral blood volume map shows increased rCBV in the arrowed area (rCBV ratio, 5.40). **d** Volume of interest (*yellow square*) for multivoxel MRS was placed over the arrowed area. **e** Spectra show pathologic spectra with normal Cho/NAA ratio as 0.72 although showing increased Cho/Cr ratio as 1.76. These findings seen on ADC map, rCBV map, and MRS were consistent with tumor recurrence. Histopathology revealed gliosarcoma

or more, the score was 1; if less than 2.10, the score was 0. If Cho/Cr$\geq$1.29 and Cho/NAA$\geq$1.06, the score was 1; if less than these thresholds, it was 0.

The accuracy, sensitivity, specificity, positive predictive value, and negative predictive value of the multiparametric scoring system are summarized in Table 4. With a scoring system threshold value of 2, the overall accuracy of 93.3% was statistically significant ($p<0.05$).

In two of five radiation change cases (case 2 and 5), the total score was 0. Also, in two of five cases of radiation

Table 4 Sensitivity, specificity, PPV, and NPV of each parameter and scoring system in differentiation of two entities.

PPV positive predictive value, *NPV* negative predictive value, *NS* no significance

	Threshold	Accuracy	Sensitivity	Specificity	PPV	NPV	*p* value
ADC ratio	1.30	13/15	9/10	4/5	9/10	4/5	<0.01
rCBV ratio	2.10	13/15	9/10	4/5	9/10	4/5	<0.01
Cho/Cr	1.29	12/13	10/10	2/3	10/11	2/2	<0.01
Cho/NAA	1.06	11/13	9/10	2/3	9/10	2/3	<0.05
Cho/Cr and Cho/NAA	1.29, 1.06	11/13	9/10	2/3	9/10	2/3	<0.05
Scoring system	2	14/15	10/10	4/5	10/11	4/4	<0.005

injury (case 1 and 3), in which MRS was considered uninterpretable, the total score was 0 or 1, showing radiation necrosis. Only one case of radiation injury using the described criteria (case 4) was misclassified as tumor progression with the total score of 3 (Fig. 2).

In seven of ten cases of tumor progression, the total score was 3, and in the remaining three cases (cases 11, 12, and 15), the total score was 2.

Discussion

In this small pilot study, combining results from multiple physiologic MR studies (DWI, PWI, and MRS) using a multiparametric scoring system improved accuracy of differentiation of tumor progression and radiation change beyond that of any single method alone. Each physiologic MR technique has limitations including a variable rate of technical failure most often encountered with MRS. In two cases of radiation injury (cases 1 and 3) in which MRS was uninterpretable, the diagnosis was correctly categorized by both ADC ratio and rCBV ratio. Furthermore, three cases of tumor progression (cases 11, 12, and 15) that were incorrectly classified by either rCBV ratio (case 11), ADC ratio (case 12), or Cho/Cr+Cho/NAA (case 15) alone were correctly categorized by the combined score from all physiologic MR parameters. Thus, these results suggest that this multiparametric scoring system can potentially offset an incorrect classification based on any single physiologic MR parameter.

In tumors, ADC values are typically highest in cystic or necrotic areas compared with solid tumor components that reflect tumor cellularity [4]. There are a few reports in which DWI has been useful for discriminating recurrent tumor from radiation necrosis [3, 5, 6]. Recurrent tumors have been shown to have significantly lower ADC values (mildly restricted diffusion) compared with radiation change, possibly related to the increased cellularity of tumors [3, 5, 6]. Application of ADC ratio may improve differentiation [3, 5].

From the study of Hein et al., of 18 patients with high-grade glioma after completion of radiation therapy, ADC ratios above 1.62 only occurred in radiation necrosis, while ratios lower than this threshold only occurred in recurrent tumor. In comparison the threshold value of our cases was lower and might be the result of the proportion of high-versus low-grade glioma in each series due to the small number of cases in each series.

Relative CBV determined by DSC is potentially useful since it reflects underlying microvasculature and angiogenesis [7, 8]. Several types of imaging sequences have been used for DSC in characterizing tumors [9]. We used the PRESTO sequence which has a slightly decreased susceptibility sensitivity compared with gradient echo (GRE) single-shot echo-planar imaging. PRESTO pulse sequences

are thus not as affected by susceptibility artifacts, better enabling perfusion scans throughout the entire brain including the skull base [10–12] and in the presence of post-operative changes, such as hemorrhage or metallic surgical implants. Manka et al. reported that dynamic susceptibility imaging with PRESTO was feasible at 3 T, and additionally the contrast agent dose could be reduced to 0.1 mmol/kg because of stronger susceptibility effects at higher magnetic field strengths [11].

Sugahara et al. examined 20 patients with suspected recurrent glioma by using dynamic susceptibility GRE MR perfusion and concluded that normalized rCBV ratio (rCBV of enhancing lesion to rCBV of contralateral white matter) of more than 2.6 suggested tumor progression, and a ratio less than 0.6 suggested a non-neoplastic contrast-enhancing tissue [7]. In our series, mean rCBV ratios were 1.82 ± 0.79 in radiation change and 3.33 ± 1.16 in tumor progression, and optimal threshold was calculated at 2.10. These differences again may reflect our small patient series as well as use of PRESTO versus GRE EPI sequences.

MRS metabolite ratios have been used to differentiate recurrent tumor from post-therapeutic change. Cho/Cr ratio reflects increases in choline and is sensitive in detecting tumor growth. There are several published threshold Cho/Cr values for discrimination of the two entities [3, 13–18] that include 1.11 [13], 1.50 [14], 1.71 [15], 1.79 [16], 1.80 [17], and 2.0 [18].

Cho/NAA ratio, which combines the increase of choline with depression of NAA, is also sensitive in detecting tumor growth. Previous studies found a combination of Cho/Cr and Cho/NAA to be useful for optimal discrimination of the two entities. Plotkin et al. investigated the value of single-voxel MRS at 3 T in 25 patients (six low-grade and 19 high-grade gliomas) with suspected recurrent glioma based on MR imaging after treatment with radiation therapy. A combined threshold of Cho/Cr (1.11) or Cho/NAA (1.17) or both resulted in 89% sensitivity and 83% specificity for identifying tumor [13]. We applied a combination of Cho/Cr (1.29) and Cho/NAA (1.06) to reduce false-negative results. This resulted in 84.6% accuracy, 90% sensitivity, and 67% specificity ($p<0.01$, Chi-square test).

Our results include one case of radiation necrosis (case 4), which was misclassified as tumor progression due to low ADC ratio, high rCBV ratio, and high Cho/Cr and Cho/NAA (Fig. 2). It has been reported that low ADC values may be seen in radiation necrosis, possibly reflecting the early necrosis with abundant polymorphonuclear leukocytes and that heterogeneity on DWI images are usual findings in radiation necrosis [6]. It has also been suggested that the cause of increased rCBV in radiation necrosis may be due to vascular changes within irradiated brain tissue, such as aneurysmal formation, telangiectasia, vascular elongation, and a remarkable proliferation of endothelial cells, especially in the capillary bed [7]. Furthermore, high Cho/NAA

and Cho/Cr values have been attributed to radiation-induced inflammation, demyelination, and gliosis [19]. Therefore, our findings in case 4 may reflect inflammatory and vascular changes of post-radiation therapy. However, in this case, with only single-voxel MRS, low levels of all metabolites relative to normal or tumor tissue due to cellular injury or cell death may be present and difficult to detect even though ratios of remaining tissue signal reflect metabolic ratios similar to tumor thus resulting in misclassification. This can be assessed through quantitative MRS measures of metabolite concentrations but this is not done in clinical studies. It can also be suggested in multivoxel spectroscopy if signal from lesion voxels is significantly lower than surrounding tissue.

Positron emission tomography (PET) technique is also currently in use. Fluorodeoxyglucose (FDG) PET studies have shown that areas of radiation injury have lower glucose metabolism than normal brain tissue because they have lower cellular attenuation [20]. A previous PET review reported the sensitivity of ^{18}F-FDG PET to be 81–86% and the specificity to be 40–94% in differentiating late-delayed radiation injury from recurrent high-grade glioma [21]. Recent study have shown that a series of 117 post-radiotherapy patients demonstrated a sensitivity of 96% and specificity of 77% in distinguishing recurrent tumor from radiation necrosis when MRI and PET image were coregistered [22]. False-positive FDG uptake can be observed in inflammatory processes and subclinical seizure activity. In particular, radiation injury can activate repair mechanisms or lead to inflammatory activity, which increases glucose metabolism [21].

Limitations

There are a number of limitations to this study. Since this is a retrospective study there are no consistent MRS parameters used across the different studies. MRS was performed using either multi- and/or single-voxel technique, and some studies were done with short TE, while others were done with intermediate to long TE values. Tim et al. assessed the diagnostic value of 3-T single-voxel MRS with short versus intermediate TE in grading cerebral glioma in 35 patients and showed that choline/creatine and choline/NAA ratios were significantly lower at short TE compared with those obtained at longer TE [23]. In addition, MRS was done post-contrast in all cases to better localize the area of enhancing abnormality for performing the single-voxel MRS positioning or for selecting the best voxel for analysis with multivoxel MRS. Not all subjects had technically interpretable results on all three physiologic studies. There were a small number of patients meeting inclusion criteria for this study, which results in a small sample size from which it is difficult to draw firm conclusions. The

pathologic types of tumors were very heterogeneous as were the types of treatment delivered. Of importance is the fact that there was no true gold standard for determination of the final diagnosis of tumor progression versus radiation damage. A histological result from biopsy of the suspicious lesion was done in only a limited number of our patients. Instead, a combined set of MR and clinical criteria was used to make this determination for the majority of patients. Finally, the single observer who evaluated the ADC values, rCBV, and MRS data was not blinded to the results from the other imaging studies and clinical data.

Because of these limitations, the results of this study should be considered a preliminary pilot investigation. Further validation is needed with a larger number of cases. However, the fact that there were a number of cases in which results from the different physiologic MR studies differed and that the multiparametric scoring system yielded the correct diagnosis in nearly all cases is very encouraging. In fact, there was only one case that yielded a misdiagnosis using the scoring system, and in this case all three physiologic imaging studies were concordant and suggested an incorrect diagnosis. Thus, our results suggest that final diagnosis between tumor progression and post-radiation damage using the multiparametric scoring system may improve diagnostic accuracy as well as increase the level of confidence of the final diagnosis compared with imaging studies alone or any single physiologic MR study.

Conclusion

This pilot study of post-treatment glioma patients with suspicion for tumor progression versus post-radiation change suggests that using a multiparametric scoring system combining results from multiple physiologic MR techniques (DWI, DSC, and MRS) may improve overall diagnostic accuracy beyond that of each single technique alone. The technique may better differentiate glioma progression from post-radiation damage, and further investigation of this approach is warranted.

References

1. Mullins ME, Barest GD, Schaefer PW, Hochberg FH, Gonzalez RG, Lev MH (2005) Radiation necrosis versus glioma recurrence: conventional MR imaging clues to diagnosis. AJNR Am J Neuroradiol 26:1967–1972
2. Kumar AJ, Leeds NE, Fuller GN, Van Tassel P, Maor MH, Sawaya RE, Levin VA (2000) Malignant gliomas: MR imaging

spectrum of radiation therapy- and chemotherapy induced necrosis of the brain after treatment. Radiology 217:377–384

3. Zeng QS, Li CF, Liu H, Zhen JH, Feng DC (2007) Distinction between recurrent glioma and radiation injury using magnetic resonance spectroscopy in combination with diffusion-weighted imaging. Int J Radiat Oncol Biol Phys 78:151–158

4. Lam WW, Poon WS, Metreweli C (2002) Diffusion MR imaging in glioma: does it have any role in the pre-operation determination of grading of gliomas? Clin Radiol 57:219–225

5. Hein PA, Eskey CJ, Dunn JF, Hug EB (2004) Diffusion-weighted imaging in the follow-up of treated high-grade gliomas: tumor recurrence versus radiation therapy. AJNR Am J Neuroradiol 25:201–209

6. Asao C, Korogi Y, Kitajima M et al (2005) Diffusion-weighted imaging of radiation-induced brain injury for differentiation from tumor recurrence. AJNR Am J Neuroradiol 26:1455–1460

7. Sugahara T, Korogi Y, Tomiguchi S, Shigematsu Y, Ikushima I, Kira T, Liang L, Ushio Y, Takahashi M (2000) Post therapeutic intra axial brain tumor: the value of perfusion-sensitive contrast-enhanced MR imaging for differentiating tumor recurrence from nonneoplastic contrast-enhancing tissue. AJNR Am J Neuroradiol 21:901–909

8. Cha S, Knopp EA, Johnson G, Litt A, Glass J, Gruber ML, Lu S, Zagzag D (2000) Dynamic contrast-enhanced T2*-weighted MR imaging of recurrent malignant gliomas treated with thalidomide and carboplatin. AJNR Am J Neuroradiol 21:881–890

9. Sugahara T, Korogi Y, Kochi M, Ushio Y, Takahashi M (2001) Perfusion sensitive MR imaging of gliomas: comparison between gradient-echo and spin-echo echo-planar imaging techniques. AJNR Am J Neuroradiol 22:1306–1315

10. Liu G, Sobering G, Duyn J, Moonen CT (1993) A functional MRI technique combining principles of echo-shifting with a train of observations (PRESTO). Magn Reson Med 30:764–768

11. Manka C, Träber F, Gieseke J, Schild HH, Kuhl CK (2005) Three-dimensional dynamic susceptibility-weighted perfusion MR imaging at 3.0T: feasibility and contrast agent dose. Radiology 234:869–877

12. van Gelderen P, Grandin C, Petrella JR, Moonen CT (2000) Rapid three-dimensional MR imaging method for tracking a bolus of contrast agent through the brain. Radiology 216:603–608

13. Plotkin M, Eisenacher J, Bruhn H, Wurm R, Michel R, Stockhammer F, Feussner A, Dudeck O, Wust P, Felix R, Amthauer H (2004) 123I-IMT SPECT and 1HMR-spectroscopy at 3.0T in the differential diagnosis of recurrent or residual gliomas: a comparative study. J Neurooncol 70:49–58

14. Ando K, Ishikura R, Nagami Y, Morikawa T, Takada Y, Ikeda J, Nakao N, Matsumoto T, Arita N (2004) Usefulness of Cho/Cr ratio in protonMR spectroscopy for differentiating residual/recurrent glioma from non-neoplastic lesions. Nippon Igaku Hoshasen Gakkai Zasshi 64:121–126

15. Zeng QS, Li CF, Kai Z, Liu H, Kang XS, Zhen JH (2007) Multivoxel 3D proton MR spectroscopy in the distinction of recurrent glioma from radiation injury. J Neurooncol 84:63–69

16. Rock JP, Hearshen D, Scarpace L, Croteau D, Gutierrez J, Fisher JL, Rosenblum ML, Mikkelsen T (2002) Correlations between magnetic resonance spectoroscopy and image-guided histopathology, with special attention to radiation necrosis. Neurosurgery 51:912–920

17. Weybright P, Sundgren PC, Maly P, Hassan DG, Nan B, Rohrer S, Junck L (2005) Differentiation between brain tumor recurrence and radiation injury using MR spectroscopy. AJR Am J Roentgenol 185:1471–1476

18. Lichy MP, Henze M, Plathow C, Bachert P, Kauczor HU, Schlemmer HP (2004) Metabolic imaging to follow stereotactic radiation of gliomas the role of 1H MR spectroscopy in comparison to FDG PET and IMT-SPECT. Rofo 176:1114–1121

19. Schlemmer HP, Bachert P, Herfarth KK, Zuna I, Debus J, van Kaick G (2001) Proton MR spectroscopic evaluation of suspicious brain lesions after stereotactic radiotherapy. AJNR Am J Neuroradiol 22:1316–1324

20. Di Chiro G, Oldfield E, Wright DC (1988) Cerebral necrosis after radiotherapy and/or intraarterial chemotherapy for brain tumors: PET and neuropathologic studies. AJR Am J Roentgenol 150:189–197

21. Langleben DD, Segall GM (2000) PET in differentiation of recurrent brain tumor from radiation injury. J Nucl Med 41:1861–1867

22. Wang SX, Boethius J, Ericson K (2006) FDG-PET on irradiated brain tumor: ten years' summary. Acta Radiol 47:85–90

23. Kim JH, Chang KH, Na DG, Song IC, Kwon BJ, Han MH, Kim K (2006) 3T H-MR spectroscopy in grading of cerebral gliomas: comparison of short and intermediate echo time sequences. AJNR Am J Neuroradiology 27:1412–1418